An Algebraic Method to Synthesize Specified Modal Currents in Ladder Resonators: Application to Non-circular Birdcage Coils

Nicola De Zanche[a] and Klaas P. Pruessmann[b]

a. Division of Medical Physics, Department of Oncology, University of Alberta, Edmonton, Canada

b. Institute for Biomedical Engineering, University of Zurich and ETH Zurich, Zurich, Switzerland

Published in

Magnetic Resonance in Medicine

DOI: 10.1002/mrm.25503

Correspondence Address: Nicola De Zanche
Division of Medical Physics
Department of Oncology
University of Alberta
11560 University Avenue
Edmonton, Alberta
T6G 1Z2 Canada

E-mail: dezanche@ieee.org
Phone: + 1-780-989-8155
Fax: + 1-780-432-8615

Abstract

Purpose:

Detectors such as birdcage coils often consist of networks of coupled resonant circuits that must produce specified magnetic field distributions. In many cases, such as quadrature asymmetric insert body coils, calculating the capacitance values required to achieve specified currents and frequencies simultaneously is a challenging task that previously had only approximate or computationally-inefficient solutions.

Theory and Methods:

A general algebraic method was developed that is applicable to linear networks having planar representations such as birdcage coils, TEM coils, and numerous variants of ladder networks. Unlike previous iterative or approximate methods, the algebraic method is computationally efficient and determines current distribution and resonant frequency using a single matrix inversion. The method was demonstrated by specifying irregular current distributions on a highly elliptical birdcage coil at 3T.

Results

Measurements of the modal frequency spectrum and transmit field distribution of the two specified modes agrees with the theory. Accuracy is limited in practice only by how accurately the matrix of self and mutual inductances of the network is known.

Conclusion

The algebraic method overcomes the inability of the existing inductance equalization method to account for all elements of the inductance matrix and the inability to accommodate modal currents that are not (co)sinusoidal.

Keywords

network synthesis; mesh analysis; ladder networks; ladder coil tuning; cyclic coupled networks; asymmetric birdcage coils

Introduction

Radio frequency resonators, or "coils", used in *in-vivo* magnetic resonance measurements create B_1 fields and, reciprocally (1), allow signal reception by producing controlled distributions of currents on conductive segments that are located at specific spatial locations. These typically inductive branches are connected by capacitive elements (discrete lumped capacitors or the capacitance between conductive surfaces separated by a dielectric) to yield resonant circuits with, often, several resonant frequencies and corresponding current distributions, or "modes". Coil design aims to achieve resonance modes with currents that produce specified magnetic field distributions at the desired frequencies, often with constraints on mode degeneracy (multiple modes sharing the same resonant frequency) and coupling. In this work the network's geometry and desired currents are assumed to be determined by independent design choices or optimizations. We present a general method to determine the capacitance values required to produce a desired modal structure in circuits such as 2-D ladder networks (2-6) or cyclic structures such as the birdcage coil (7) (including variants such as the dome resonator (8)), the TEM coil (9), ring resonator (10), and magnetron (11,12).

Traditional implementations of these networks are typically highly symmetric which greatly simplifies the analysis of modal structure. Symmetry often allows modal currents to be deduced by inspection and frequencies have relatively simple, closed-form expressions from the electrical parameters of the network. Symmetry also ensures that the same value of capacitance will be repeated at multiple locations, and therefore there are only a few unknown capacitances that must be determined. The same is not true for asymmetric structures, or in general networks for which simple geometric operations such as rotation do not yield an identical network. Because the number of unknown capacitances can be several times larger for asymmetric networks than for their symmetric counterparts, tuning asymmetric networks is a considerable challenge which has previously been approached by computationally-inefficient iterative optimizations (13), or by using approximate methods. One such method, mesh inductance equalization (14,15), ignores coupling between non-adjacent meshes and is limited to distributions of currents where electrical phase is incremented by a constant amount between successive meshes. In a quadrature coil these assumptions often result in non-degenerate modes and this must be corrected to avoid loss of performance (16). Correction can be achieved using a heuristic method where the resonant frequency of each isolated mesh is adjusted (17),

introducing a further approximation because this method cannot control the resulting field patterns. The need for producing optimized transmit field homogeneity using asymmetric resonators has recently intensified with the increasing applications of non-proton hyperpolarized techniques (18), which require uniform excitation so that the available, non-replenishable polarization can be used as efficiently as possible. Consequently, since approximate methods do not provide optimal fields they cannot be used to design volume transmitters for hyperpolarized applications.

The goal of the present work is to provide a rational approach to the design of general ladder networks by using mesh analysis and an efficient algebraic method for calculating lumped reactances. The primary applications, and motivations are the variants of the ubiquitous birdcage coil that have been modified from the original circular cylindrical shape (7) to increase sensitivity or to meet mechanical constraints. These asymmetric variants include contours such as the rectangle (19), ellipse (14), quartic (17), oval of Cassini (13), and flat-bottomed ovals for table-top applications (18,20). The method's range of application readily extends to the active field of multichannel transmit/receive arrays constructed of separate elements or integrated such as the birdcage coil in array mode (21,22).

Theory

In electrical circuit analysis it is often advantageous to express Kirchhoff's equations in terms of *mesh* quantities rather than the familiar nodal quantities (23). Mesh analysis is possible only for planar networks (23), i.e., those that can be represented on a plane without crossing branches. Many ladder resonators used in magnetic resonance, including the birdcage coil (24), can be represented as planar networks and have been analyzed using this technique (2,25).

Leifer's matrix formulation (25) rearranges Kirchhoff's mesh equations into the generalized eigenvalue equation (26)

$$\mathbf{E}\,\nu = \lambda \mathbf{L}\,\nu\,, \qquad (1)$$

which gives the angular frequencies, ω (related to the eigenvalues by $\lambda = \omega^2$), and eigenvectors (containing mesh currents $\nu = \left(J_1 \ldots J_N\right)^T$) of the resonant modes of the ladder network. Here **L** is the matrix of the meshes' mutual and self inductances, and **E** is the *elastance* matrix which contains the electrical coupling terms, i.e., the inverse of capacitance. Parasitic electric coupling is considered negligible, or is lumped into an equivalent capacitance. For a given geometry the

inductance matrix is typically determined by measurement or simulation, while the matrix **E** is unknown and must be determined based on the desired current distributions and resonant frequencies.

We also make the implicit assumption that network losses are negligible (27-29) compared to stored electromagnetic energy, which is equivalent to saying that equivalent series resistances are much smaller than the reactances of the network or that the quality factors (Q) of the resonant modes are much greater than unity (e.g., $Q > 20$). When this assumption is valid the standard perturbation approach can be used to determine the reduction in resonant frequency due to losses (30, §8.8) relative to the lossless case.

Consider an N-element birdcage coil that lacks the typical rotational symmetry, while retaining symmetry along the central transverse plane (Figure 1a). The elastance matrix **E** of Ref. (25) can be generalized as

$$\mathbf{E} = \left\{ E_{ij} \right\} = \begin{pmatrix} \frac{2}{C_{11}} + \frac{1}{C_{12}} + \frac{1}{C_{1N}} & -\frac{1}{C_{12}} & 0 & \cdots & -\frac{1}{C_{1N}} \\ -\frac{1}{C_{12}} & \frac{2}{C_{22}} + \frac{1}{C_{12}} + \frac{1}{C_{23}} & -\frac{1}{C_{23}} & \cdots & 0 \\ 0 & -\frac{1}{C_{23}} & \frac{2}{C_{33}} + \frac{1}{C_{23}} + \frac{1}{C_{34}} & -\frac{1}{C_{34}} & \vdots \\ \vdots & & & \ddots & -\frac{1}{C_{N,N-1}} \\ -\frac{1}{C_{1N}} & \cdots & 0 & -\frac{1}{C_{N,N-1}} & \frac{2}{C_{NN}} + \frac{1}{C_{1N}} + \frac{1}{C_{N,N-1}} \end{pmatrix} \quad (2),$$

where C_{ii} are the end-ring capacitances and C_{ij} are the rung capacitances (i.e., shared capacitances between meshes) shown in Figure 1b. Such networks of linear, time-invariant, passive, and bilateral lumped elements are reciprocal (23) thus ensuring that both **E** and **L** are symmetric.

Elements in the anti-diagonal corners of **E** are indicative of the cyclic nature of the birdcage network (24), which may not be the case in other forms of ladder network. The null elements off the 3 main diagonals and corners arise from allowing connections only between adjacent elements in the birdcage. Other structures may have more or fewer finite elements in **E**

depending on the topology. For example, in 2-D ladder networks (2,6) each loop can have shared capacitances with four or more adjacent meshes, but meshes at opposite edges are not connected and the terms in the corners of **E** are zero. Structures such as the TEM coil (9), free-element resonator (31), ring resonator (10), surface coil arrays and high-pass 2-D networks (6), where coupling is primarily inductive, will also lack the electric coupling terms adjacent to the diagonal of **E**, unless an equivalent network is generated using the standard tee or pi equivalent circuits of a transformer (32,33).

<Figure 1>

Solutions of the generalized eigenvalue equation

The inductance matrix **L** is real, symmetric, and by invoking energy conservation, while excluding the possibility of perfect magnetic coupling, we can also ensure that it is positive definite (34) and therefore invertible. Since the elastance matrix **E** is symmetric by construction, it ensures that the generalized eigenvalue problem of Eq. (1) is equivalent to finding the eigenvalues of a symmetric matrix (26). The *pair* (**L**, **E**) is said to be symmetric even though $\mathbf{D} = \mathbf{L}^{-1}\mathbf{E}$ is not necessarily symmetric, but only similar to a symmetric matrix. We can therefore be certain that for any physically-realizable ladder network the eigenvalues λ and eigenvectors ν (current distributions) are real and they form an orthonormal basis. These properties ensure the existence of N orthogonal resonance modes that can be excited individually, even if degenerate, without transferring signal or energy. Multiport resonators such as quadrature coils or arrays therefore provide an independent sensitivity pattern at each port which can be used, e.g., to improve SNR or to provide sensitivity encoding.

In a standard birdcage coil **L** and **E** are also *circulant* matrices, i.e., having rows obtained by progressively shifting the elements of a single row vector (35). The numerous properties of circulant matrices and how they apply to standard circular birdcage coils have been discussed in detail in Ref. (25). Specifically, circulant systems have two eigenvectors with the sinusoidal and cosinusoidal current distributions (modes of azimuthal order or periodicity equal to 1) needed to produce uniform transverse fields in circular birdcage and TEM coils. These same distributions can also produce uniform fields in a birdcage coil whose rungs lie on a surface obtained from the circle by a suitable conformal mapping (13,14). Appropriate additional symmetries (e.g., symmetry about the anti-diagonals of **L** and **E**) can ensure that the (co)sinusoidal modes are also degenerate.

In such birdcage coils obtained by a conformal mapping lacking rotational symmetry, we must still produce (co)sinusoidal currents to create uniform magnetic fields even though **L** is not circulant. One option is to choose $\mathbf{D} = \mathbf{L}^{-1}\mathbf{E}$ such that it is a suitable circulant matrix (it is not necessary for the factor matrices to be circulant for their product to be circulant) (35). However, as shown in the Appendix, this approach is equivalent to specifying all eigenvalues and eigenvectors of the system and consequently **E** will contain non-zero elements throughout. Restoring a circulant system is therefore not a practical approach to design ladder networks where the topology (circuit layout and connections) are predetermined.

Specifying the desired modes

Fortunately, by specifying only the desired eigenvalues and eigenvectors the remaining degrees of freedom can be exploited to give **E** the desired structure of Eq. (2). We begin by writing a system of equations using one generalized eigenvalue equation (1) for each of the network's modes for which we wish to specify a current distribution and resonant frequency. In the case of a quadrature birdcage coil we specify the two orthogonal (uniform field) linear modes:

$$\begin{pmatrix} \mathbf{E}v_A \\ \mathbf{E}v_B \end{pmatrix} = \lambda \begin{pmatrix} \mathbf{L}v_A \\ \mathbf{L}v_B \end{pmatrix}, \tag{3}$$

where λ has been factored out to indicate that mode A and mode B will be degenerate so they can be excited simultaneously at the same frequency. For other coil designs (e.g., multiport networks used for arrays) Eq. (3) would contain as many additional copies of Eq. (1) as needed to specify all the required modes (up to N).

The modal currents in an asymmetric birdcage coil are typically chosen to maintain the high field homogeneity that is achieved with a standard circular coil. For rung positions determined using the conformal mapping approach (13,14) the eigenvectors are simply

$$v_A = \begin{pmatrix} 1 \\ \cos(2\pi/N) \\ \vdots \\ \cos(2\pi(N-1)/N) \end{pmatrix}, \; v_B = \begin{pmatrix} 0 \\ \sin(2\pi/N) \\ \vdots \\ \sin(2\pi(N-1)/N) \end{pmatrix}, \tag{4}$$

while for other rung arrangements the optimal currents must be determined by other means.

Current distributions optimized for desired field distributions

Standard circular birdcage coils are well-known to require sinusoidally-distributed currents to maximize field homogeneity (7,36). Other coil shapes or conductor placements will require a separate determination of current intensities different from those of Eq. (4) to achieve the desired field pattern before network synthesis methods can be applied. Many examples exist in the literature that either make use of, or could benefit from optimization of modal current distributions, including elliptical coils with uniformly-spaced rungs (37), the "quartic" coil (17), biplanar coils (38,39), and various versions of open coils (40-44).

Optimization will typically be performed on rung or, in general ladder networks, branch currents (labeled I_j in Figure 1b), since these currents are directly responsible for the magnetic fields. Field simulations can in many cases be as simple as quasi-static 2D calculations using the Biot-Savart law. More realistic simulations could include the effects of finite rung length and the presence of currents in the end rings.

The branch currents must be transformed to mesh currents (J_j in Figure 1b) before the algebraic method presented here can be applied. In network theory (see Section 3.6 of Ref. (23)) the mesh current vector is obtained from the branch current vector by multiplication with the *tie-set* matrix. For birdcage coils it can readily be observed that if the end-ring meshes are neglected (which is equivalent to assuming that the end-ring currents are zero) this transformation (Eq. (4) of Ref. (40)) has rank N–1 and therefore cannot be uniquely inverted unless further assumptions are made. One method of achieving this conversion for birdcage coils is to restrict the solution space of the inversion to mesh current distributions that have a zero mean.

Formulating the solution by rearranging the matrix equation

The linear system of Eq. (3) may then be expanded element-by-element and re-written with the unknown (non-zero) elements of **E** extracted from the two diagonals and top right corner, and arranged in a column vector $e_G = \left(E_{11}, E_{22}, \cdots E_{NN}, E_{12}, E_{23}, \cdots E_{N,N-1}, E_{1N}\right)^T$ of length $2N$ (this takes into account the symmetry of **E** without repeating elements). Equation (3) then becomes

$$\mathbf{G}e_G = b\,, \tag{5}$$

where b is the right-hand side of Eq. (3) and the matrix **G** has dimensions $2N \times 2N$ and contains the elements of v_A and v_B suitably rearranged:

$$\mathbf{G}=\begin{pmatrix} v_{A1} & 0 & 0 & \cdots & 0 & v_{A2} & 0 & \cdots & 0 & v_{AN} \\ 0 & v_{A2} & 0 & \cdots & 0 & v_{A1} & v_{A3} & 0 & \cdots & 0 \\ 0 & & & & \vdots & 0 & & \ddots & & \vdots \\ \vdots & & & \ddots & 0 & \vdots & & v_{A,N-2} & v_{AN} & 0 \\ 0 & 0 & \cdots & 0 & v_{AN} & 0 & \cdots & 0 & v_{A,N-1} & v_{A1} \\ v_{B1} & 0 & 0 & \cdots & 0 & v_{B2} & 0 & \cdots & 0 & v_{BN} \\ 0 & v_{B2} & 0 & \cdots & 0 & v_{B1} & v_{B3} & 0 & \cdots & 0 \\ 0 & & & & \vdots & 0 & & \ddots & & \vdots \\ \vdots & & & \ddots & 0 & \vdots & & v_{B,N-2} & v_{BN} & 0 \\ 0 & 0 & \cdots & 0 & v_{BN} & 0 & \cdots & 0 & v_{B,N-1} & v_{B1} \end{pmatrix}. \tag{6}$$

Although this system contains an equal number of equations and unknowns, it is not guaranteed to provide a unique solution since the rank of **G** is not full. The existence of a solution will depend on whether the particular network's topology and inductance matrix can support the specified current distributions (see examples below). Finding a *unique* solution of Eq. (5) requires reducing the number of unknowns by introducing relationships such as setting at least one of the capacitors to a predetermined value. For example, in the case of a hybrid birdcage coil (45) the ratio of end-ring to rung capacitance is a free parameter that must be set independently by the designer.

Formulating the solution using Kronecker products

We now present an alternative method of solution that can be readily generalized to network topologies other than the birdcage without manually working out the system of equations from which the **G** matrix above is created. While this makes it easier to implement in software, the solution requires a greater number of constraints to enforce on **E** the desired structure of Eq. (2). This method relies on the use of Kronecker products and the *vec* operator (see, e.g., Chapter 16 of Ref. (26)) which takes the elements of a matrix and rearranges them in a column vector. The Kronecker product between matrices $\mathbf{A}=\{a_{ij}\}$ and **B** is non-commutative and is denoted $\mathbf{A}\otimes\mathbf{B}$. The row and column dimensions of the product matrix are the product of the respective dimensions of the original matrices and the elements are defined by

$$\mathbf{A}\otimes\mathbf{B}=\begin{pmatrix} a_{11}\mathbf{B} & \cdots & a_{1N}\mathbf{B} \\ \vdots & \ddots & \vdots \\ a_{M1}\mathbf{B} & \cdots & a_{MN}\mathbf{B} \end{pmatrix}. \tag{7}$$

A general linear system of equations in the unknowns contained in matrix **X**, and elements in matrices **A**, **B** and **C**, can be written equivalently as

$$\mathbf{AXC} = \mathbf{B} \quad \text{or} \quad \left(\mathbf{C}^T \otimes \mathbf{A}\right) x = b\,, \tag{8}$$

where $x = \text{vec}(\mathbf{X})$ and $b = \text{vec}(\mathbf{B})$. By re-arranging the system of Eq. (3) as two-column matrices

$$\left(\mathbf{E}v_A \quad \mathbf{E}v_B\right) = \lambda\left(\mathbf{L}v_A \quad \mathbf{L}v_B\right) \quad \text{or} \quad \mathbf{EV} = \lambda\mathbf{LV}\,, \tag{9}$$

where $\mathbf{V} = \left(v_A \quad v_B\right)$, the property of Eq. (8) may be applied with the substitutions $\mathbf{A} = \mathbf{I}_N$ (the identity matrix of order *N*), $\mathbf{B} = \lambda\mathbf{LV}$, $\mathbf{C} = \mathbf{V}$ and unknowns $\mathbf{X} = \mathbf{E}$. In the resulting expression,

$$\mathbf{K}e_K = b\,, \tag{10}$$

the vector *b* is identical to that in Eq. (5) by virtue of the *vec* operator, while $e_K = \text{vec}(\mathbf{E})$ and $\mathbf{K} = \mathbf{V}^T \otimes \mathbf{I}_N$ is a $2N \times N^2$ matrix. As anticipated, the left-hand side contains N^2 unknowns compared to $2N$ of the method of the previous section because it does not contain any *a priori* information regarding the null elements and symmetry of **E**. While this missing information will need to be added, the advantage of the formulation of Eq. (10) over that of Eq. (5) lies in the simplicity and flexibility with which the problem can be coded in matrix calculation software such as MATLAB (The Mathworks, Natick, MA, USA), thus avoiding the manual generation of matrix **G** of Eq. (6) which is prone to human error.

Imposing constraints and solving

Both formulations described above require the introduction of constraints in order for these underdetermined systems to have a unique solution. The constraints result from considerations such as the symmetry of the **E** matrix with respect to the main diagonal, which is a consequence of the reciprocity of linear networks. Elements of **E** may also be set to zero to reflect the ladder network's topology as in the hybrid birdcage coil (45) example of Eq. (2). Additional symmetries and repetitions may occur due to symmetries in the coil topology or geometry, and are a powerful tool to test the stability of the solution as a function of the number of unknowns (i.e., solving with or without accounting for the additional symmetries should give the same result). Finally, in the case of a hybrid birdcage coil (45) the ratio between capacitance in the end ring to

that in the rung capacitors must also be chosen independently (e.g., by imposing a fixed ratio between one of the end-ring capacitances and one of the rung capacitances) prior to solution. Consequently, constraints will take one of two forms: either to impose a linear relationship (e.g., equality) between given elements of **E**, or to impose a specified value on an element. The former can be implemented by adding a row below b and **G** or **K** for each desired equality, such as

$$\begin{pmatrix} \boxed{\begin{matrix}\mathbf{G}\\ \text{or}\\ \mathbf{K}\end{matrix}} \\ 0 \;\cdots\; 0 \;\; 1 \;\; 0 \;\cdots\; 0 \;\; -1 \;\; 0 \;\cdots\; 0 \end{pmatrix} e_{G,K} = \begin{pmatrix} b \\ 0 \end{pmatrix} \tag{11}$$

where the 1 and −1 are in the columns that correspond to two elements of $e_{\mathrm{G,K}}$ that must be equal (or appropriate scalars for other proportionalities). Similarly, a specific value, e_0, can be specified by additional rows containing a single unity entry in this manner:

$$\begin{pmatrix} \boxed{\begin{matrix}\mathbf{G}\\ \text{or}\\ \mathbf{K}\end{matrix}} \\ 0 \;\cdots\; 0 \;\; 1 \;\; 0 \;\cdots\; 0 \end{pmatrix} e_{G,K} = \begin{pmatrix} b \\ e_0 \end{pmatrix}. \tag{12}$$

The special case of $e_0 = 0$ can also be dealt with by removing the element of $e_{\mathrm{G,K}}$ and the corresponding column of **G** or **K**. Such constraints can be used in any number or combination as necessary to produce a system of the form $\mathbf{H}e_{G,K} = b_h$, where **H** and b_h contain as many rows with the form of Eqs. (11) and (12) as needed. Once the **H** matrix has full column rank the system is readily solved by matrix inversion or Moore-Penrose generalized inverse (pseudoinverse), $\hat{e} = \mathbf{H}^{+} b_h$. Capacitances of the hybrid birdcage coil are obtained from the resulting elements of **E** by applying the definitions in Eq. (2), or from the corresponding definition of **E** for other network topologies.

Existence of a solution and comparison of the formulations

Given a desired set of eigenvectors, the existence of a solution is not guaranteed, but depends on the circuit topology (allowed shape of **E**) and geometry (entries in **L**). A full exploration of these relationships is beyond the scope of this work, but the example provided below illustrates that

unconventional current distributions are possible with standard birdcage ladder network structures.

When a solution exists, the choice of formulation will have a small but negligible effect on the result because the methods using the **G** or **K** matrices result in systems with different numbers of unknowns (the Kronecker product method yields a system with many more equations than with the rearranged matrix **G**, with a correspondingly larger number of constraints required to specify zero elements and symmetry in **E**). The differences are due to the fact that the pseudoinverse produces a least-squares solution (i.e., finds a vector $\hat{e}$ that minimizes $\left\|\mathbf{H}\hat{e} - b_h\right\|$), which in general may not meet the specified constraints exactly because each term in the norm is weighted equally. The constraint equations are not given preferential treatment, and therefore the corresponding terms in the norm have the same likelihood as those terms corresponding to actual unknown capacitances of being tweaked by the pseudoinverse in the process of finding the least-squares solution. Weighting the rows of the system unevenly (26) may be used to improve how well the constraints are satisfied.

In our experience, observed differences in capacitance values between the formulations using the **G** or **K** matrices are well below 1%, and thus negligible compared to the uncertainty with which the **L** matrix is known (> 1% in the example below). Even in absence of uncertainty in **L** these differences can always be considered negligible since at typical in-vivo NMR frequencies controlling impedances to an accuracy of 1% is a challenging task. The method by which the matrices are generated and the constraints are specified therefore does not have a substantial influence on the accuracy of the solution.

A note on the order of complexity of linear networks

In the preceding analysis we have assumed that *N* equations are sufficient to model the resonant behaviour of an *N*-section birdcage coil, which is indeed true if we neglect the co-rotating end-ring mode (25). For a general network, however, the minimal number of equations required to describe it must be determined so that all possible modes can be accounted for. Extra equations should not be introduced to avoid an ill-conditioned system. This optimal number of equations is referred to as the network's *order of complexity* (34,46-48) and coincides with the dimension of the state space of the dynamical system that the network represents (48).

The order of complexity of networks can be determined by laborious reduction of all the equations resulting from Kirchhoff's circuit laws to a system that contains only linearly independent equations. The rank of such a system corresponds to the order of complexity. A more insightful method of determining the order of complexity is to use topological analysis of the network using graph theory, leading to the formula (34)

$$N = N_L + N_C - \left(N_{CL} + N_{LC}\right) \tag{13}$$

where N_L is the number of inductors, N_C is the number of capacitors, N_{CL} is the number of independent capacitive loops and N_{LC} is the number of independent inductive cutsets. The latter are, respectively, loops that consist only of capacitors and cutsets that contain only inductors, and represent redundancies that can be eliminated using Kirchhoff's voltage and current laws. Although the presence of losses (e.g., resistors that represent equivalent losses due to biological loading in MRI coils) is typically negligible in the modal analysis of Eq. (1), when determining the network's order of complexity losses must be considered (47) since they can alter the latter two terms of Eq. (13).

The general hybrid birdcage coil, and low-pass and high-pass limiting cases can be analyzed similarly to the lumped-element model of the magnetron (11,12,34). The resulting order of complexity is N+1, as expected, which includes N–1 modes that are typically pair-wise degenerate in a coil with appropriate symmetry (e.g., standard circular coils). We note also that the slight difference in topology between the low-pass birdcage and the magnetron results approximately in a doubling in the number of nonzero resonant frequencies (11).

Specific examples of the order of complexity of birdcage-like structures with $N = 3$ (48), $N = 4$ (28) and $N = 5$ (34, p.166) have been analyzed in the literature and confirm the expression above. Other, more complex structures such as the multiple-end-ring birdcage (49), or dual-tuned versions incorporating traps (50,51), will lead to higher orders of complexity and may not be modelled with sufficient accuracy by considering only the N or N+1 modes that are observed in a standard birdcage.

Design Process for Asymmetric Birdcage Coils

An example of how the algebraic method can be integrated into the design process for asymmetric birdcage coils is summarized by the flowchart in Figure 2. The inputs are the operating frequency of the resonator and the shapes of the RF shield and coil former which are

typically specified by independent geometrical constraints. The first step is to decide the number and positions of the coil's rungs, which are then used to determine the current intensities (eigenvectors ν) that result in sufficiently uniform transverse magnetic fields, and the inductance matrix **L**. The algebraic method is then used to calculate the elastance matrix **E** from which the capacitances are obtained. A final check is performed using Eq. (1) to ensure that the desired modes are not too close to the remaining modes of the network. If they are, the process must be repeated with different locations and/or number of rungs.

<Figure 2>

Birdcage with Sinusoidal Modal Currents: The Cassinian coil revisited

An initial verification of the proposed method was performed by comparing its predicted capacitances to those obtained by full-wave (method of moments) numerical simulation of a 3T head coil designed on a Cassinian oval former (13). Since the complete inductance matrix was unavailable for this coil, the higher-order mutual inductances (those between non-adjacent meshes) were assumed to be zero. This assumption is also made in the mesh inductance equalization method of Refs. (14,15) that is used as a standard for comparison of the resulting capacitance values.

The capacitances obtained for the Cassinian head coil using the method of moments simulation are compared in Table 1 with those obtained using self and nearest-neighbour mutual inductances by the mesh inductance equalization method of Refs. (14,15), and with those obtained using the new algebraic method of the previous sections. The main differences are in C_{22} which are due likely to an $L_{2,15}$ term that is not negligible due to the proximity of these meshes, and in the rung capacitances due to the fact that C_{12} is assumed to be a short in the latter 2 methods. Note that reactance is proportional to 1/C and therefore the large differences in rung capacitances are not necessarily significant. There is excellent agreement between the mesh inductance equalization method and the present method, confirming its validity under the assumption of zero higher-order mutual inductances. It is expected that if this unrealistic assumption were removed there would be more substantial differences between the second and third row of Table 1due to mesh inductance equalization's inability to utilize the additional information.

<Table 1>

Birdcage Coil in Array Mode

An additional validation of the algebraic method was performed on published data for a birdcage coil operated in array mode (21,22). Ideally a birdcage array has N degenerate modes each corresponding to a current in only one mesh, i.e., the vectors v of Eqs. (4) form the identity matrix. However, as noted in Ref. (28) this perfect degeneracy is impossible to achieve because a birdcage coil does not have an **E** matrix with elements off the main three diagonals that would be required to cancel the effects of its full **L** matrix.

A mesh inductance matrix for an 8-rung coil was generated from the data in Table 3 of Ref. (28) by applying Eq. (12) of Ref. (25). The Kronecker product method above was used with constraints on off-diagonal elements of **E** specified according to Eq. (12). Two sets of constraints on the frequencies were compared. In the first system the desired frequency of all eight modes was set to 63.8 MHz, resulting in capacitance values of 47.9 pF and 66.0 pF for the rungs and end-rings, respectively, compared to 49.2 pF and 59.8 pF according to the results of Ref. (28). In this solution, the frequencies of most modes are close to the mean value of 63.11 MHz with a standard deviation of 1.0 MHz except for the mode at 72.44 MHz (63.99±0.46 MHz and 76.01 MHz, respectively, in Ref. (28)) in which all mesh currents are equal. This is the counter-rotating end-ring mode and its frequency should be left free since the end-ring modes do not produce the primarily transverse magnetic fields that are required for imaging in a standard cylindrical magnet.

A second matrix system was therefore set up with the row corresponding to the end ring mode removed, resulting in capacitances of 51.3 pF and 58.1 pF, respectively. The resulting mode frequencies, 63.84±0.47 MHz and 77.17 MHz, are within 1.5% of those of Ref. (28).

If the number of rungs is greater than eight, we have observed that the additional finite off-diagonal terms in **L** cannot be compensated for with an **E** matrix constrained as above, and therefore the number of modes whose frequency must be allowed to be unconstrained must be increased (e.g., 3 modes for 16 rungs). These limitations in the number of degenerate modes of the birdcage coil in array mode (i.e., number of useful modes < N) make its performance inferior to that of standard arrays that use preamplifier decoupling (52) except in situations where a limited number of channels is sufficient (e.g., in transmit arrays (22)).

Methods

The theory introduced above was further verified by constructing a 12-element elliptical birdcage coil with dimensions roughly suitable for wrist imaging (Figure 3). The coil rungs (5-mm-diameter copper rods 126 mm in length) were positioned according to Ref. (14) on an elliptical surface having major and minor diameters of 90 and 60 mm, respectively. Rungs were optionally split into two sections of equal length (joined by a 2 mm PTFE spacer) to allow capacitors to be connected across the gap for a hybrid version (45). The end rings joining the extremities of the rungs were constructed by etching 10-mm-wide copper traces on fibreglass (FR4) circuit board attached to the rungs using brass screws. The birdcage network is surrounded by a concentric circular RF shield (aluminium foil on a PMMA former) 120 mm in diameter.

<Figure 3>

Current distributions

The chosen rung positions allow uniform fields to be produced with (co)sinusoidal rung currents in the *absence* of an RF shield (14), or in the presence of a confocal elliptical outer shield (53), but not with other shapes such as the 120-mm circular cylinder. Nonsinusoidal current distributions were therefore determined for the two linearly polarized modes by independently minimizing the standard deviation of the field amplitude of each mode within an elliptical region that is confocal with the coil former. This 2-D quasi-static field calculation uses the method of images (54) to account for the presence of the circular shield. The resulting rung current distributions (shown in Figure 4a) produce fields that are only slightly more homogeneous than those from the standard sinusoidal distributions. A second, more irregular set of currents was therefore chosen to test the method's ability to generate specified current distributions. The corresponding field homogeneity plots are shown in Figure 4b and c.

<Figure 4>

Tuning

The mesh inductance equalization procedure (14,15) cannot be used to determine the capacitances needed to produce non-sinusoidal currents because this method is limited to producing equal increments of electrical phase between adjacent meshes.

The inductance matrix of the shielded coil was determined similarly to Ref. (18) by populating isolated meshes or mesh pairs with 91 pF porcelain capacitors (series 100B, American Technical

Ceramics) having closely matched values (90±0.1 pF) as measured at 1 MHz with an HP4285A impedance meter (Agilent, USA). The 1 pF discrepancy between nominal and measured capacitance value is within the nominal 5% tolerance and is attributed to the manufacturing processes. For this measurement the coil rungs were ungapped copper rods and the capacitors were soldered to the appropriate locations on the end rings. Other end-ring sections were not only left open but also disconnected from the unused rungs by removing the brass screws, thus minimizing the effect of parasitic capacitances. The resulting resonant frequencies were determined using a weakly-coupled 1-cm-diameter shielded loop probe and a network analyzer (HP8753, Agilent, USA) in reflection (S_{11}) measurement mode over the frequency span between 60 and 80 MHz. Inductances were calculated using standard formulae for single or coupled resonant circuits (24,31) and values with magnitude below 2 nH were considered to be below the measurement's sensitivity and set to zero.

The algebraic method was then used as described in the Theory section to calculate the capacitances required for operation at 127.8 MHz with the three current distributions of the previous section. The (co)sinusoidal and homogeneity-optimized distributions required constraining rung capacitor C_{34} to a short circuit (infinite capacitance) to fully determine the system of equations (see Imposing constraints and solving); conversely, the irregular distributions required setting C_{23} to a short circuit. Note that if any of the other rung capacitors are shorted instead, an unphysical solution with some negative capacitance values will result.

A large number of capacitors (100B series, American Technical Ceramics, USA) with nominal values of 15, 18, 33, 39, 47, 56, and 100 pF were measured at 1 MHz using the HP4285A impedance meter and each value was recorded. Bins were created with the required number of capacitors or combinations of capacitors chosen such that their values be as close as possible to those calculated for the irregular distributions. Furthermore, maximal symmetry along the two longitudinal planes of symmetry was ensured for each value bin by using the half of the capacitors with larger values on the end ring where the cable connections are to be made, while the other half are used on the opposite end ring. The resonant frequencies were measured using weak inductive coupling and no additional capacitors were used for tuning or mode de-coupling. The inductance matrix of the unshielded coil was also measured and the algebraic method was applied with the same current distributions. For all distributions C_{34} was set to a short circuit to achieve a solution with positive capacitance values.

Bench performance measurements

An approximately elliptical container having major and minor diameters of 66 mm and 36 mm, respectively, and length 135 mm was filled with ~300 mℓ of a demineralised water solution containing 2.00 g/ℓ of NaCl and 0.77 g/ℓ of $CuSO_4 \cdot 5H_2O$ to mimic biological tissue. Loaded and unloaded quality factors (Q) were measured using a transmission measurement (S_{21}) with two loop probes weakly coupled to one of the linearly polarized modes, followed by the second mode.

Lattice baluns (56,57) were constructed to match the 50 Ω coaxial feed cables to the loaded port impedances across end-ring capacitors on meshes 1 and 10. Baluns were accurately tuned by temporarily shorting the coil-side output of the balun and adjusting the inductances to place the higher of the resulting modes at 127.8 MHz (two modes are always present due to mutual inductance in the current paths of the lattice balun even though the two inductive windings can be decoupled by placing them at right angles). Resulting return loss measurements are approximately 20 dB for both ports and isolation is 18 dB or better in loaded conditions. In unloaded conditions values are 5.5 dB and 16 dB, respectively. This level of performance was deemed acceptable (16) and therefore variable capacitors for fine tuning of frequency and isolation were not installed.

Transmit field maps

The elliptical test coil was connected for two sets of measurements with linear excitation, i.e., exciting port 1 and 10 individually while the other port is matched to a 50 Ω load. Transmit field (B_1^+) amplitude measurements were then performed on the above phantom in the central transverse plane of the coil using the double-angle method (58). Two gradient-echo images were acquired in successive experiments with nominal tip angles of 40 and 80° and T_E = 4.5 ms, T_R = 5000 ms, 110 mm FOV, 10 mm slice thickness, 96×96 matrix (reconstructed to 128×128) and one average.

Results

Tuning

The measured inductance matrix of the shielded elliptical birdcage is given in Table 2 and the capacitance values calculated with the algebraic method for the three specified current distributions are given in Table 3.

<Table 2>

<Table 3>

The resonant frequencies of the prototype coil are shown in Figure 5 in comparison to those predicted by theory using both the algebraic method and mesh inductance equalization. As expected, the algebraic method is able to achieve degenerate order-one modes for the standard (co)sinusoidal current distributions while mesh inductance equalization (14,15) is not because it cannot account for inductances between non-adjacent meshes. For the irregular current distribution, the separation between uniform modes and the nearest higher-order mode is slightly worse in the prototype than predicted by the algebraic method but within acceptable limits (~10 MHz) given the high Q factors.

<Figure 5>

For the unshielded coil, however, it was found that for the (co)sinusoidal and optimized current distributions there are higher-order modes very close (<5 MHz) to the desired frequency which preclude the use of this unshielded resonator when quality factors are realistic. We speculate that this is due to the fact that without the shield the inductive coupling is stronger and more asymmetric between non-nearest-neighbour meshes than with the shield present (e.g., facing meshes such as nos. 4 and 10 have stronger coupling than nos. 1 and 7). The resulting solutions deviate from the standard obtained from circulant systems both in the distribution of modal frequencies and currents. Alterations to the coil geometry such as increasing the number of meshes or distributing the rungs in a different manner may provide an improved modal distribution as could a reduction in ellipticity or introduction of a closely-fitting shield.

Performance

Quality factor results in Table 4 indicate, consistently with other oval coils (13,14,53), a higher efficiency (55) for the mode that produces a B_1 field parallel to the short axis of the coil. The tip angle maps shown in Figure 6 are in good qualitative agreement with the simulated maps of

Figure 4. Discrepancy in the field map of the horizontal mode is attributed to the asymmetric loading due to the placement of the matching circuits.

<Table 4>

<Figure 6>

Conclusion

An algebraic network synthesis method has been developed to calculate the capacitance values required to resonate MR ladder coils that have varying degrees of symmetry. Specified modal current distributions and frequencies are achieved simultaneously, thus allowing multiport applications such as quadrature operation. The algebraic method is based on mesh equations and is applicable to linear networks that have planar representations such as birdcage coils, TEM coils, and numerous variants of ladder networks. Computational efficiency is assured by the single inversion of a matrix whose rank is of the same order of magnitude as the order of complexity of the ladder network. Unlike iterative (13) or approximate (14,17) methods, the algebraic method optimizes current distribution and resonant frequency simultaneously, and its accuracy is limited in practice only by how accurately the inductance matrix of the network is known. The new method is consistent with the existing inductance equalization method, and furthermore overcomes its inability to account for all elements of the inductance matrix and the inability to accommodate modal currents that are not (co)sinusoidal. This algebraic method has been applied with success to an asymmetric insert birdcage body coil for ^{3}He imaging (18) and in this work to a highly elliptical wrist-size coil with an irregular current distribution. The test prototype shows excellent agreement with the theory in terms of the modal frequency spectrum and transmit field distribution of the two specified modes. Future applications include more complex designs such as four-ring and other multiply-tuned birdcage coils.

Acknowledgements

The authors acknowledge insightful discussions with Drs. David Brunner, Philip Davis and Mark Leifer. Technical assistance from Messrs. Paul Lüthi, Aldo Rossi, and Stephen Wheeler is also gratefully acknowledged.

Appendix

By choosing $\mathbf{D} = \mathbf{L}^{-1}\mathbf{E}$ such that it is a suitable circulant matrix, the properties of circulant matrices then allow us to write $\mathbf{D} = \mathbf{F}^{H}\Lambda\mathbf{F}$, where $\mathbf{\Lambda}$ is a diagonal matrix containing the eigenvalues of **D**, superscript *H* indicates the conjugate (Hermitian) transpose, and **F** is the Fourier matrix whose elements are the coefficients of the discrete Fourier transform. By definition, **F** contains the eigenvectors of **D** and therefore defines *all* of the modal currents. The eigenvalues in $\mathbf{\Lambda}$ may be chosen independently in order to place each mode at the desired frequency. For example, undesired modes that do not produce uniform fields can be kept well separated from the two modes that do. Calculation of **E** is then straightforward,

$$\mathbf{E} = \mathbf{L}\mathbf{F}^{H}\Lambda\mathbf{F}\,. \tag{A1}$$

However, since both **L** and **D** are likely to have non-zero elements throughout, **E** will generally yield a dense matrix that does not have the limited envelope or sparsity (tridiagonal plus the two corners) described by Eq. (2). These additional non-zero elements correspond to elastances that cannot be physically inserted into the birdcage ladder network without introducing additional capacitive connections (33,59,60) between non-adjacent rungs. These additional connections create further inductively-coupled meshes that increase the dimension of the problem (see also A note on the order of complexity of linear networks), i.e., additional meshes with self and mutual inductances. Even a careful choice of eigenvalues will not restore the desired structure because the restriction that is imposed by the choice of eigenvectors (the complete matrix **F**) limits the available degrees of freedom.

References

1. Hoult DI. The Principle of Reciprocity in Signal Strength Calculations - A Mathematical Guide. Concepts in Magnetic Resonance 2000;12(4):173-187.
2. Ballon D, Meyer KL. Two-Dimensional Ladder Network Resonators. Journal of Magnetic Resonance, Series A 1994;111(1):23-28.
3. Meyer KL, Ballon D. A 3 × 3 Mesh Two-Dimensional Ladder Network Resonator for MRI of the Human Head. Journal of Magnetic Resonance, Series B 1995;107(1):19-24.
4. Meyer KL, Kim K, Li T, Tulipano PK, Lee K-M, Delapaz R, Hirsch J, Ballon D. Sensitivity-enhanced echo-planar MRI at 1.5T using a 5 × 5 mesh dome resonator. Magn Reson Med 1996;36(4):606-612.
5. Molyneaux DA, Haq Qureshi A. Arbitrary placement array coil system. IEEE Transactions on Magnetics 1997;33(5):4104-4106.
6. Voss HU, Ballon DJ. High-Pass Two-Dimensional Ladder Network Resonators for Magnetic Resonance Imaging. IEEE Transactions on Biomedical Engineering 2006;53(12):2590.
7. Hayes CE, Edelstein WA, Schenck JF, Mueller OM, Eash M. An Efficient, Highly Homogeneous Radiofrequency Coil for Whole-Body NMR Imaging at 1.5 T. J Magn Reson 1985;63(3):622-628.
8. Srinivasan R, Liu H. Evaluation of a "True" Dome Quadrature Head Coil for Functional Imaging. In: Proceedings of the International Society for Magnetic Resonance in Medicine, 3rd annual meeting; 1995; Nice. p 973.
9. Vaughan JT, Hetherington HP, Otu JO, Pan JW, Pohost GM. High Frequency Volume Coils for Clinical NMR Imaging and Spectroscopy. Magn Reson Med 1994;32(2):206-218.
10. Solymar L. Rotational resonance of magnetoinductive waves: Basic concept and application to nuclear magnetic resonance. J Appl Phys 2006;99(12):123908.
11. Lin P, Flanders H. Natural frequencies of cyclic linear networks. IEEE Transactions on Circuit Theory 1971;18(5):551-554.
12. Mansfield P, McJury M, Glover P. High Frequency Cavity Resonator Designs for NMR. Meas Sci Technol 1990;1(10):1052-1059.
13. De Zanche N, Yahya A, Vermeulen FE, Allen PS. Analytical approach to noncircular section birdcage coil design: Verification with a Cassinian oval coil. Magn Reson Med 2005;53(1):201-211.
14. Leifer MC. Theory of the Quadrature Elliptic Birdcage Coil. Magn Reson Med 1997;38(5):726-732.
15. Keller JS, Lo Vetri J, Barberi EA, Rutt BK. Tuning of the Quadrature Elliptic Birdcage Coil-Part I: Mesh Inductance Equalization. In: Proceedings of the ISMRM, 7th Annual Meeting; 1999; Philadelphia. International Society for Magnetic Resonance in Medicine. p 2057.
16. Tropp J, Derby K. The loss of signal to noise due to imperfect isolation between the channels of a quadrature nuclear magnetic resonance probe. Review of Scientific Instruments 1991;62(11):2646-2653.
17. Riauka TA, De Zanche NF, Thompson RB, Vermeulen FE, Capjack CE, Allen PS. A Numerical Approach to Non-Circular Birdcage RF Coil Optimization: Verification With a Fourth-Order Coil. Magn Reson Med 1999;41(6):1180-1188.

18. De Zanche N, Chhina N, Teh K, Randell C, Pruessmann KP, Wild JM. Asymmetric quadrature split birdcage coil for hyperpolarized ^{3}He lung MRI at 1.5T. Magn Reson Med 2008;60(2):431-438.
19. Vullo T, Pascone R, Mancuso R, Zipagan R, Cahill PT. Transmission line analysis of noncylindrical birdcage resonators. Magn Reson Imag 1994;12(5):785-797.
20. Luedeke K, Röschmann P, Overweg J, Schulz V. A novel asymmetric RF Body-Coil. In: Proceedings 11th Scientific Meeting, International Society for Magnetic Resonance in Medicine; 2003 10-16 July; Toronto. p 2352.
21. Leussler C, Stimma J, Röschmann P. The Bandpass Birdcage Resonator Modified as a Coil Array for Simultaneous MR Acquisition. In: Proceedings of the International Society for Magnetic Resonance in Medicine, 5th annual meeting; 1997; Vancouver. p 173.
22. Alagappan V, Nistler J, Adalsteinsson E, Setsompop K, Fontius U, Zelinski A, Vester M, Wiggins GC, Hebrank F, Renz W, Schmitt F, Wald LL. Degenerate mode band-pass birdcage coil for accelerated parallel excitation. Magn Reson Med 2007;57(6):1148-1158.
23. Choudhury DR. Networks and Systems: Wiley; 1988.
24. Tropp J. Mutual Inductance in the Bird-Cage Resonator. J Magn Reson 1997;126(1):9-17.
25. Leifer MC. Resonant Modes of the Birdcage Coil. J Magn Reson 1997;124(1):51-60.
26. Harville DA. Matrix algebra from a statistician's perspective. New York: Springer-Verlag; 1997. 630 p.
27. Pascone RJ, Garcia BJ, Fitzgerald TM, Vullo T, Zipagan RT, Cahill PT. Generalized Electrical Analysis of Low-pass and High-pass Birdcage Resonators. Magn Reson Imag 1991;9:395-408.
28. Cheng YC, Eagan T, Chmielewski T, Flock J, Kang MC, Kidane T, Shvartsman S, Brown R. A degeneracy study in the circulant and bordered-circulant approach to birdcage and planar coils. Magnetic Resonance Materials in Physics, Biology and Medicine 2003;16(2):103-111.
29. Eagan TP, Cheng YCN, Kidane TK, Mathur H, Chmielewski T, Flock J, Sh MS, Brown RW. A group theory approach to RF coil design. Concepts in Magnetic Resonance Part B: Magnetic Resonance Engineering 2005;25B(1):42-52.
30. Jackson JD. Classical Electrodynamics: Wiley; 1999.
31. Wen H, Chesnick AS, Balaban RS. The design and test of a new volume coil for high field imaging. Magn Reson Med 1994;32(4):492-498.
32. Lee RF, Giaquinto RO, Hardy CJ. Coupling and decoupling theory and its application to the MRI phased array. Magn Reson Med 2002;48(1):203-213.
33. Wu B, Qu P, Wang C, Yuan J, Shen GX. Interconnecting L/C components for decoupling and its application to low-field open MRI array. Concepts in Magnetic Resonance Part B: Magnetic Resonance Engineering 2007;31B(2):116-126.
34. Guillemin EA. Synthesis of Passive Networks: Wiley; 1957.
35. Davis PJ. Circulant Matrices, second edition. New York: Chelsea Publishing; 1994.
36. Jin J. Electromagnetic Analysis and Design in Magnetic Resonance Imaging. New York: CRC Press; 1999.

37. Li CS, Collins CM, Dardzinsky BJ, Chin C, Smith MB. A Method to Create an Optimum Current Distribution and Homogenous B_1 Field for Elliptical Birdcage Coils. Magn Reson Med 1997;37:600-607.
38. Forbes LK, Crozier S, Doddrell DM. Calculating current densities and fields due to shielded bi-planar radio-frequency coils. Meas Sci Technol 1998;9(9):1609.
39. Roberts DA, Insko EK, Bolinger L, Leigh JS. Biplanar Radiofrequency Coil Design. Journal of Magnetic Resonance, Series A 1993;102(1):34-41.
40. Ballon D, Graham MC, Miodownik S, Koutcher JA. A 64MHz Half-Birdcage Resonator for Clinical Imaging. J Magn Reson 1990;90:131-140.
41. Gasson J, Summers IR, Fry ME, Vennart W. Modified birdcage coils for targeted imaging. Magn Reson Imag 1995;13(7):1003-1012.
42. Oh CH, Kim SK, Yang YJ, Ahn CB. Novel Type of Quadrature Breast RF Coil with a Ladder Structure. In: Proceedings 4th Scientific Meeting, International Society for Magnetic Resonance in Medicine; 1998; Sydney. p 2025.
43. Hockett FD, Wallace KD, Schmieder AH, Caruthers SD, Pham CTN, Wickline SA, Lanza GM. Simultaneous Dual Frequency ^{1}H and ^{19}F Open Coil Imaging of Arthritic Rabbit Knee at 3T. Medical Imaging, IEEE Transactions on 2011;30(1):22-27.
44. Yahya A, De Zanche N, Allen PS. A dual-tuned transceive resonator for $^{13}C\{^{1}H\}$ MRS: two open coils in one. NMR in Biomedicine 2013;26(5):533-541.
45. Tropp J. The hybrid bird cage resonator. In: Society for Magnetic Resonance in Medicine, 11th annual meeting; 1992 August, 1992; Berlin. p 4009.
46. Bryant PR. The order of complexity of electrical networks. Proceedings of the IEE - Part C: Monographs 1959;106(10):174-188.
47. Bers A. The Degrees of Freedom in RLC Networks. IRE Transactions on Circuit Theory 1959;6(1):91-95.
48. Kuh ES, Rohrer RA. The state-variable approach to network analysis. Proceedings of the IEEE 1965;53(7):672-686.
49. Murphy-Boesch J, Srinivasan R, Carvajal L, Brown TR. Two Configurations of the Four-Ring Birdcage Coil for ^{1}H Imaging and ^{1}H-Decoupled ^{31}P Spectroscopy of the Human Head. Journal of Magnetic Resonance, Series B 1994;103(2):103-114.
50. Matson GB, Vermathen P, Hill TC. A practical double-tuned $^{1}H/^{31}P$ quadrature birdcage headcoil optimized for ^{31}P operation. Magn Reson Med 1999;42(1):173-182.
51. Shen GX, J.F.Wu, Boada FE, Thulborn KR. Experimentally Verified, Theoretical Design of Dual-Tuned, Low-Pass Birdcage Radiofrequency Resonators for Magnetic Resonance Imaging and Magnetic Resonance Spectroscopy of Human Brain at 3.0 Tesla. Magn Reson Med 1999;41(2):268-275.
52. Roemer PB, Edelstein WA, Hayes CE, Souza SP, Mueller OM. The NMR Phased Array. Magn Reson Med 1990;16(2):192-225.
53. De Zanche N, Allen PS. Sensitivity Calculations and Comparisons for Shielded Elliptical and Circular Birdcage Coils. Magn Reson Med 2002;47:364-371.
54. Sommerfeld A. Electrodynamics. New York: Academic Press; 1952.
55. Wen H, Denison TJ, Singerman RW, Balaban RS. The Intrinsic Signal-to-Noise Ratio in Human Cardiac Imaging at 1.5, 3, and 4 T. J Magn Reson 1997;125:65-71.
56. Frankel S. Reactance Networks for Coupling Between Unbalanced and Balanced Circuits. Proc IRE 1941;29:486-493.

57. Mispelter J, Lupu M, Briguet A. NMR probeheads for biophysical and biomedical experiments: theoretical principles & practical guidelines. London: Imperial College Press; 2006.
58. Stollberger R, Wach P. Imaging the Active B_1 Field in Vivo. Magn Reson Med 1996;35(2):246-251.
59. Jevtic J. Ladder Networks for Capacitive Decoupling in Phased-Array Coils. In: Proceedings of the International Society for Magnetic Resonance in Medicine, 9th annual meeting; 2001; Glasgow, UK. p 17.
60. von Morze C, Tropp J, Banerjee S, Xu D, Karpodinis K, Carvajal L, Hess CP, Mukherjee P, Majumdar S, Vigneron DB. An eight-channel, nonoverlapping phased array coil with capacitive decoupling for parallel MRI at 3 T. Concepts in Magnetic Resonance Part B: Magnetic Resonance Engineering 2007;31B(1):37-43.

Tables

capacitance[pF]	C_{11}	C_{22}	C_{33}	C_{44}	C_{55}	C_{12}	C_{23}	C_{34}	C_{45}
optimized (13)	35.99	35.44	32.93	29.87	28.19	300.2	276.4	355.0	522.3
method of Refs. (14,15)	35.60	31.65	32.80	29.36	28.18	∞	1827	427.4	266.7
algebraic method	35.63	31.67	32.81	29.39	28.19	∞	1939	430.8	267.4

Table 1: End-ring (C_{11}-C_{55}) and rung (C_{12}-C_{45}) capacitance values for the 16-element Cassinian oval birdcage head coil (13); C_{12} is assumed to be a short in rows 2 and 3; remaining capacitances are obtained by symmetry. The rows contain, respectively, the results of numerical optimization using a full-wave numerical simulation, mesh inductance equalization (14,15) and the present algebraic method (higher-order mutual inductances set to zero). Underlined entries emphasize differences.

	1	2	3	4	5	6	7	8	9	10	11	12
1	92.41	-30.72	-5.57	-2.40						-2.40	-5.57	-30.72
2		101.0	-34.32	-5.67		-0.55			-1.14	-1.36	-2.10	-6.01
3			114.5	-37.10	-5.60			-1.14	-0.49		-1.88	-2.10
4				119.3	-37.10	-5.67	-2.40	-1.36		-1.54		-1.36

Table 2: first four rows of the elliptical coil's measured mesh inductance matrix [nH]. The remaining elements are obtained by symmetry (i.e., reflection across the dashed diagonal lines). Greyed-out cells were deemed to be below the measurement sensitivity and set to zero.

capacitance[pF]	C_{11}	C_{22}	C_{33}	C_{44}	C_{12}	C_{23}	C_{34}
(Co)sinusoidal	94.18	80.95	66.14	62.73	589.5	1105	∞
Optimized for homogeneity	93.72	81.20	66.77	65.23	220.8	783.2	∞
irregular	99.97	79.48	71.82	85.89	62.97	∞	731.4
actual used: mean	99.1	79.7	72.2	85.8	63.0	∞	∞
(nominal values)	(100)	(33+47)	(33+39)	(30+56)	(3×15+18)		

Table 3: capacitance values calculated using the algebraic method and used in the shielded elliptical coil prototype (127.8 MHz). Three sets of current patterns are considered (Figure 4a): standard sine and cosine; currents optimized for maximal homogeneity; and an irregular pattern. Numbering is according to Figure 3a and other capacitances are obtained by symmetry; ∞ indicates a short circuit; + indicates capacitors in parallel.

Coupled Mode	Unloaded *Q*	Loaded *Q*	*Q* ratio	*Efficiency*
Mesh 1	410	150	2.7	63%
Mesh 10	510	110	4.6	78%

Table 4: quality factors (*Q*) and efficiency (55) of uniform field modes at 127.8 MHz.

Figure Captions

Figure 1: a) example of a birdcage coil without rotational symmetry. The grey plane indicates the only plane of symmetry that is assumed in the analysis of the birdcage coil examples. b) section of the electrical ladder network used to model the birdcage. Sections at the far left and right are joined to introduce the required periodic boundary conditions.

Figure 2: summary of the design process for asymmetric birdcage coils. It begins by specifying the shapes of the RF shield and coil former, followed by choosing the number and location of the rungs. With these inputs the inductance matrix and optimal rung current intensities are determined, which, along with the operating frequency, provide the input to the algebraic method. If the spectral distribution of the resulting modes is not acceptable (e.g., undesired modes are too close to those specified) the process is repeated with modified positions and/or number of rungs.

Figure 3: a) the elliptical coil prototype with circular shield removed; b) cross section and mesh numbering convention.

Figure 4: a) rung current distributions considered for the shielded elliptical coil of Figure 3. The standard (co)sinusoidal distributions (dashed) would be optimal in the case of an unshielded coil or one with a confocal elliptical shield (53) and are nearly identical to those optimized for maximal field homogeneity in the presence of the circular shield (solid); irregular patterns (thicker solid) were actually used for the prototype to test the algebraic method's ability to produce specified currents. b), c) magnetic field homogeneity contours of the linearly polarized modes resulting from the irregular patterns in a) (2% intervals from amplitude at centre, empty coil, 2-D quasi-static field approximation).

Figure 5: measured and calculated resonance frequencies of the shielded elliptical birdcage coil prototype. Mode order or periodicity (defined as one half of the number of sign changes in the corresponding eigenvector) is indicated beside each calculated frequency. For the irregular current distribution used in the prototype that was built (left) the separation between uniform modes and nearest higher-order mode (arrows) is slightly worse than predicted by the algebraic method but within acceptable limits given the high *Q* factors. Mesh inductance equalization (14,15) can only be used for the standard sinusoidal and cosinusoidal current distributions (right) and unlike the algebraic method it yields order-one modes that are not degenerate (splitting indicated by dashed lines) because it cannot account for inductances between non-adjacent meshes. Consequently the prototype coil tuned using mesh inductance equalization would be unsuitable for quadrature operation.

Figure 6: normalized tip angle maps (%) obtained using the double angle method (58) in a transverse slice corresponding to the midplane of the elliptical birdcage coil. Contours at 2% intervals are overlaid. A) linear excitation at mesh 1 (horizontal B_1) and B) linear excitation at mesh 10 (vertical B_1).

a)

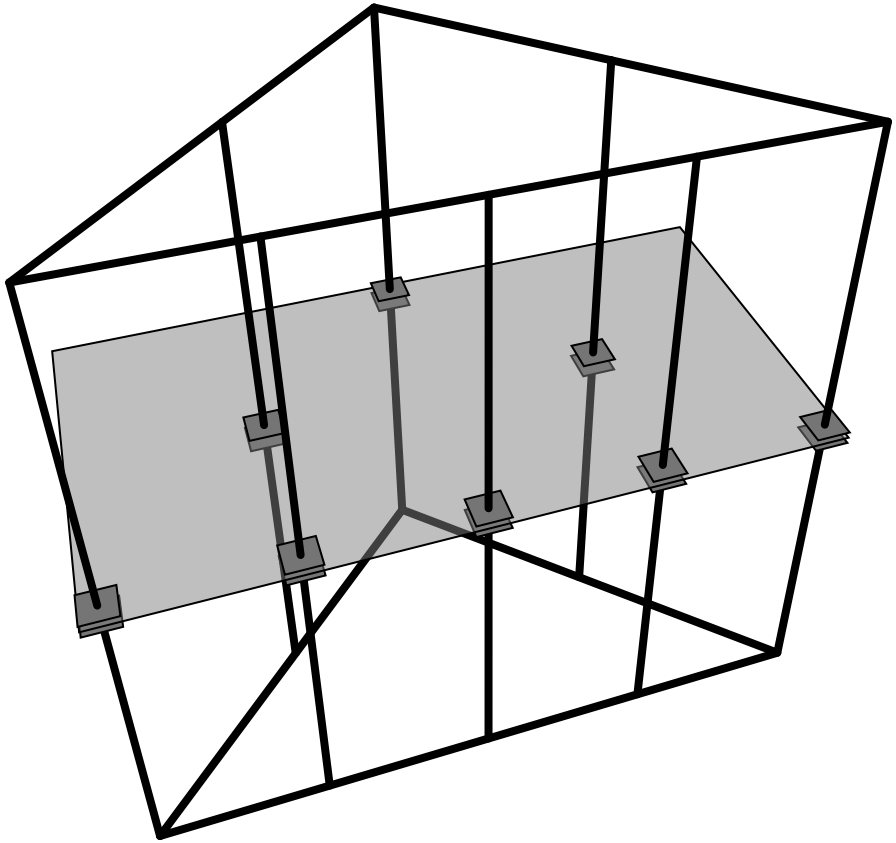

b)

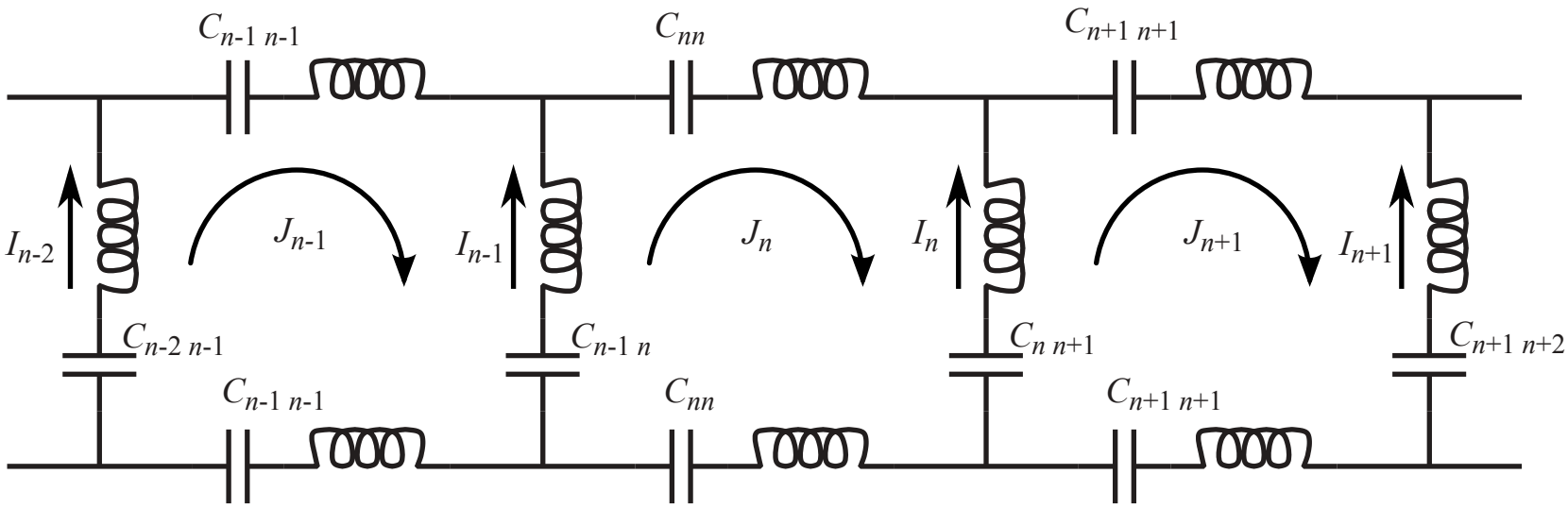
$C_{n\text{-}1\ n\text{-}1}$
C_{nn}
$C_{n+1\ n+1}$
$I_{n\text{-}2}$
$J_{n\text{-}1}$
$I_{n\text{-}1}$
J_n
I_n
J_{n+1}
I_{n+1}
$C_{n\text{-}2\ n\text{-}1}$
$C_{n\text{-}1\ n}$
$C_{n\ n+1}$
$C_{n+1\ n+2}$
$C_{n\text{-}1\ n\text{-}1}$
C_{nn}
$C_{n+1\ n+1}$

shield contour

coil former contour

choose rung number N and positions

a) optimize or specify modal rung currents v
b) measure or calculate inductance matrix **L**

algebraic method

calculate **E** (capacitances)

frequency ($\lambda=\omega^2$)

mode spectrum OK?

NO

YES

end

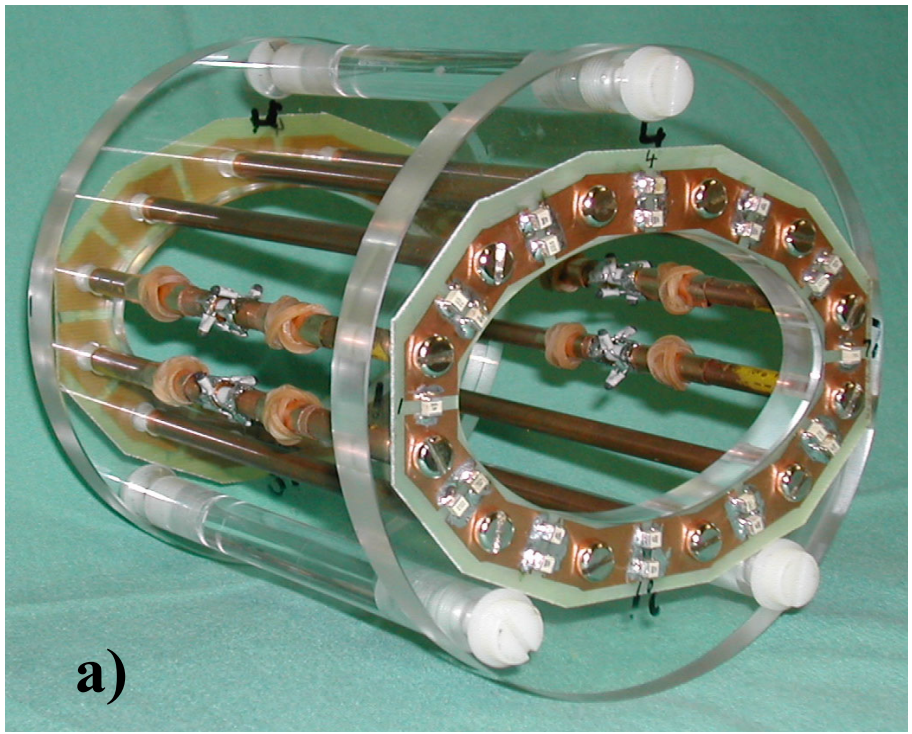
a)

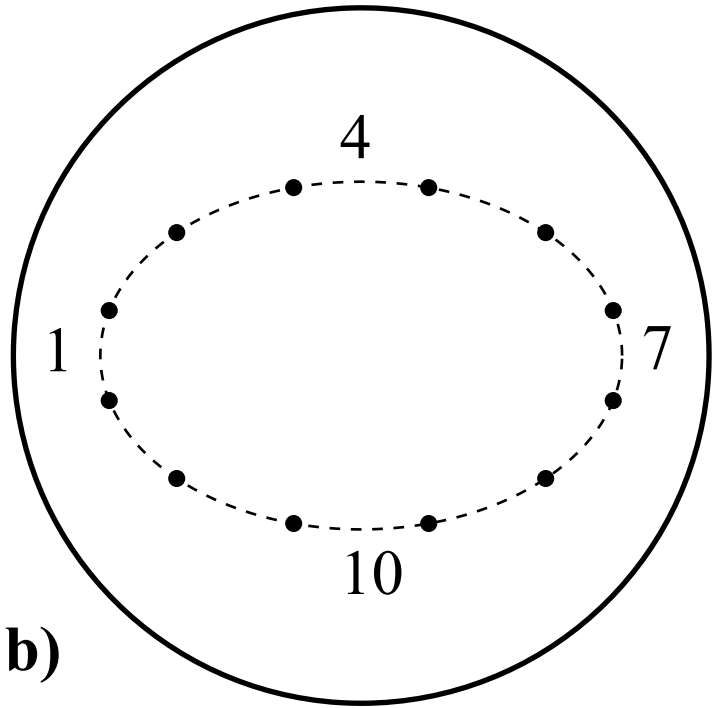
4
1
7
10
b)

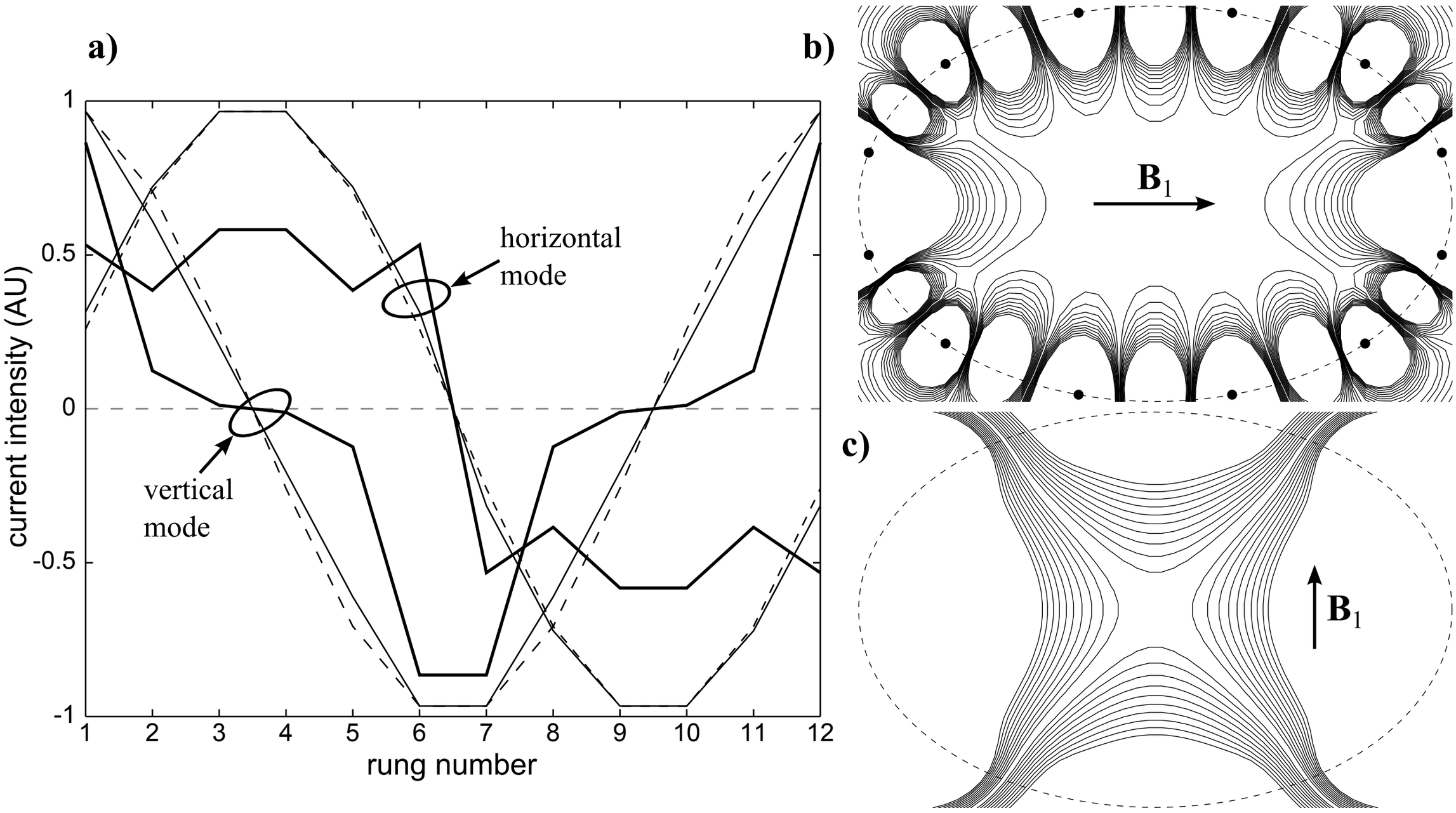
a)
b)
c)
current intensity (AU)
rung number
horizontal mode
vertical mode
B1
B1
1
0.5
0
-0.5
-1
1
2
3
4
5
6
7
8
9
10
11
12

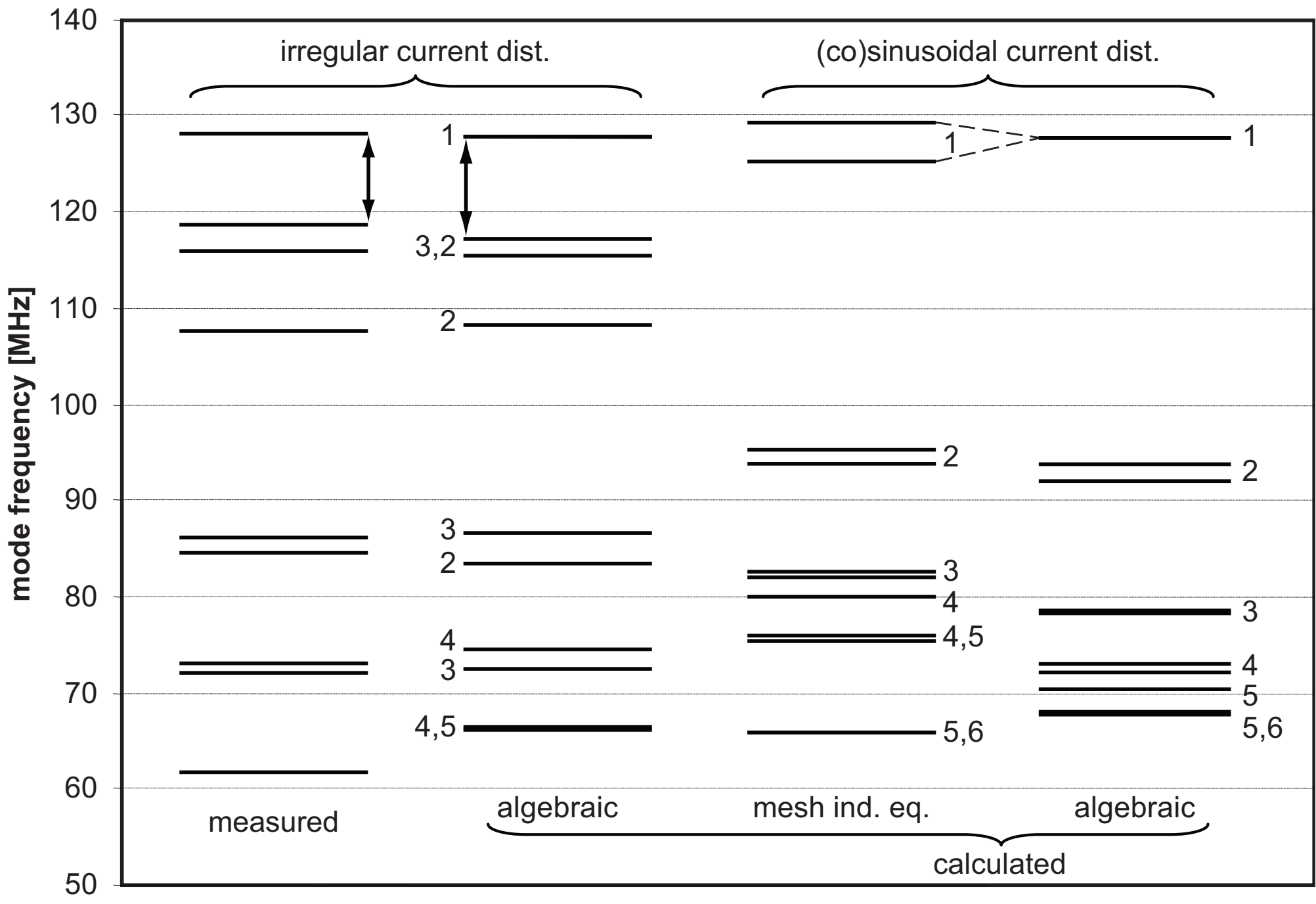
mode frequency [MHz]
140
130
120
110
100
90
80
70
60
50
irregular current dist.
(co)sinusoidal current dist.
1
3,2
2
3
2
4
3
4,5
1
1
2
3
4
4,5
5,6
2
3
4
5
5,6
measured
algebraic
mesh ind. eq.
algebraic
calculated

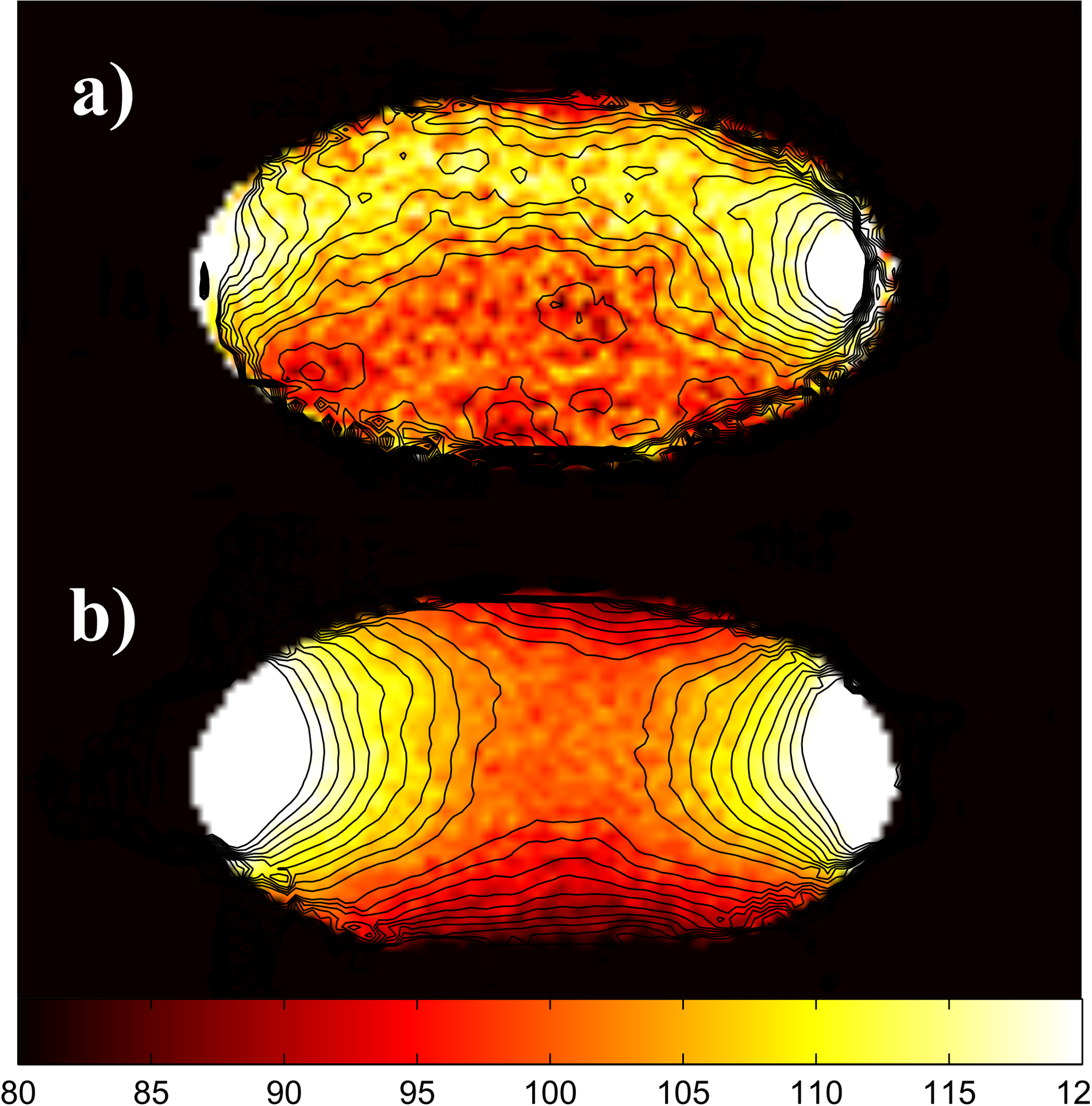
a)
b)
80
85
90
95
100
105
110
115
120